Argon and Xenon Pulsed Theta-Pinch Plasma via Optical Emission Spectroscopy

IEPC-2013-378

Presented at the 33rd International Electric Propulsion Conference,
The George Washington University, Washington, D.C., USA
October 6–10, 2013

Warner C. Meeks* and Joshua L. Rovey†
Missouri University of Science and Technology, Rolla, MO, 65409, USA

Analyses of argon and xenon spectral emission data in the IR range and estimation of electron temperatures are performed on a theta pinch test article. Estimations are based on the intensity ratio technique using collisional-radiative models. Tests performed on a pulsed xenon plasma at an energy of 80 joules, neutral back-fill pressures of 10^{-2} to 10^{-1} Torr, and vacuum discharge frequency of 460 kHz yield electron temperatures of 3.3 to 3.6 eV for argon and 6.5 to 11.3 eV for xenon integrated spectra of the first 20 μs. Spectra acquired in the UV range is used to validate the presence of dominant 2^{nd} order diffraction from singly ionized xenon transitions while minimal 2^{nd} order diffraction is observed for argon. Time-resolved electron temperature estimations are done using CCD gate widths of 250 ns. Currently, time-resolved studies of xenon show a range of electron temperatures from a minimum of 9 eV for 50 mTorr to a maximum of 92 eV for 10 mTorr. Poor single-to-noise ratios produce substantial fluctuation in intensities and thus estimation errors, while not quantified here, are assumed high for the time-resolved studies.

Nomenclature

h	= Planck's Constant
c	= vacuum speed of light
λ	= wavelength
$N_{0,e,1}$	= number density of species
$k_{e,1,2}$	= emission excitation rate coef.
α	= N_1/N_e
B_λ	= meta-stables correction factor
A^{eff}	= $A_{2,1}\eta$, effective transition probability
$A_{2,1}$	= transition probability from state $2 \rightarrow 1$
η	= escape factor

I. Introduction

Pulsed inductive plasma (PIP) devices are a type of high energy plasma source used in both research and industry.[1,2,3] In recent years, PIP devices such as the theta-pinch coil currently being investigated by the fusion and space propulsion communities utilizing deuterium and xenon, respectively, have provided promising new results in their fields.[4,5] Despite these and many other efforts to utilize PIP devices, a substantial knowledge gap remains with respect to the energy conversion processes during the early plasma formation times. All of the energy in a PIP discharge originates as stored (i.e., capacitive) electrical energy.

*Ph.D Candidate, Mechanical and Aerospace Engineering Dept., wcm994@mst.edu.
†Assistant Professor, Mechanical and Aerospace Engineering Dept., roveyj@mst.edu.

However, by the end of the device operation cycle that energy has been divided among many outlets including radiative losses (light emission, x-rays, stray capacitance/inductance), joule heating (of both the device and the gas), ill-utilized directions in bulk fluid motion (via poor containment or undesired expansion upon expulsion), and collisional processes. These collisional processes can be divided further still into numerous electronic modes, many of which do not provide a direct path to ionization. The net effect of these losses is increased ionization costs and reduced effectiveness of the device.

The broad efforts of this research are to elucidate the electric-to-particle energy conversion processes during the initial plasma formation over time scales of 10^{-8} to 10^{-6} seconds. These time-scales represent between $1/100^{th}$ and 1 discharge oscillation cycles of the Missouri Plasmoid Experiment (MPX), which has a characteristic frequency of approximately 500 kHz in vacuum. A similar set of test procedures was performed on both argon and xenon plasma and estimations of electron temperature were conducted based on separate collisional-radiative (CR) models for each gas. The work that follows is in five main parts: 1.) Description of the discharge experiment, experimental parameters, and data acquisition system. 2.) Spectral data obtained. 3.) Numerical analysis of that data and the models used. 4.) Electron temperature estimates based on those models. 5.) Discussion and conclusions.

II. Test Article and Facility

A. Theta-pinch Device

A photo of the MPX device with call-outs can be seen in Fig. 1. MPX is a theta-pinch configuration PIP test article with evacuated cylindrical dimensions of 91.5 cm length by 15.5 cm inner diameter for a volume of 1,418 cm^3 and a length-to-diameter (L/D) ratio of 5.90.[6,7] The theta-pinch coil itself, constructed from a rolled sheet of 1.5 mm thick copper, spans approximately 83% of the evacuated length at 76.2 cm and has an inner diameter of 17.8 cm. The discharge circuit consists of a single Maxwell Technologies 0.7 μF, 40 kV rated high-energy capacitor and a Perkin-Elmer GP-14B spark-gap trigger. A DC glow discharge electron source was placed at one end of the discharge chamber 15 cm away from the line-of-sight of the optical emission pick-up to assist in plasma formation and reliability. The DC source was maintained at approximately 50 volts. Figure 2 shows two typical current discharge profiles, a vacuum (i.e., no plasma) case and the other when plasma is present. Attenuation due to mutual inductance can be observed when plasma is present, and this is a well-known effect observed in similar devices.[8] This mutual inductance affects the discharge profile two-fold; 1.) it reduces the LRC time-constant and 2.) it increases the discharge frequency.

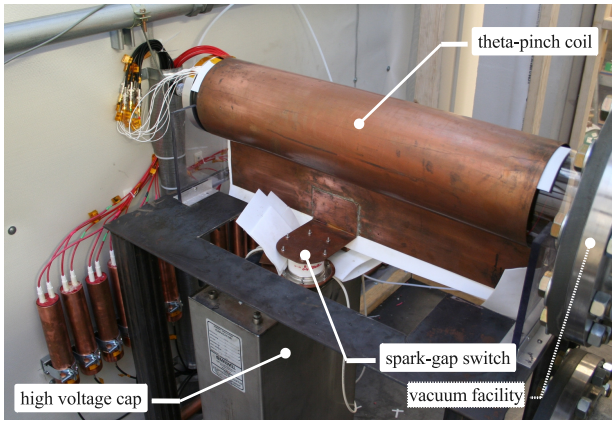

Figure 1. Missouri Plasmoid Experiment, (optical fiber not shown).

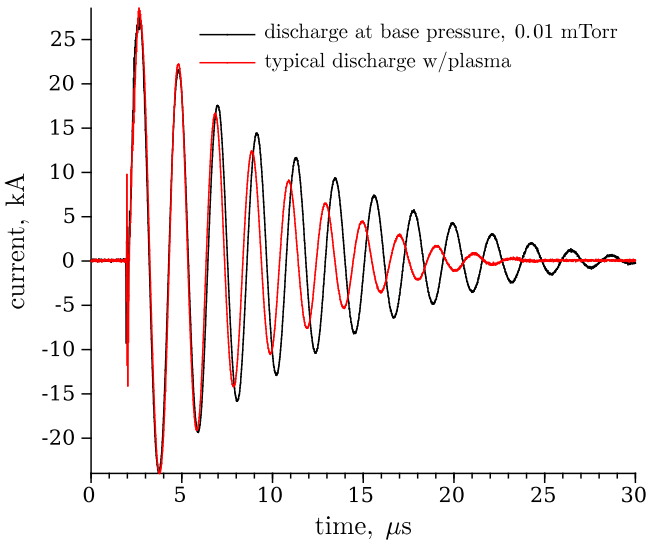

Figure 2. Typical MPX discharge profiles with and without plasma. Time zero represents when the DAQ received its trigger subsequently showing a delay of around 2 μs before capacitor discharge occurred.

B. Optical Emission Acquisition

The optical emission spectroscopy (OES) equipment used here consisted of: (1) a Princeton Instruments SP-2356 Czerny-Turner spectrometer with a 0.3 meter focal length, triple grating turret with gratings of 300, 1200, and 2400 g/mm, and a 14 mm high slit with width adjustable from 10 μm to 3 mm. Grating and slit width used here were 300 g/mm and 50 μm, respectively. (2) a PI-MAX intensified CCD camera with 1024 by 1024 pixel array. (3) a ST-133 controller with built-in PTG trigger module for repetitive (used in this work) or sequential external triggering. Light emission was transmitted from the experiment to the spectrometer slit via a 7.5 meter long, 200 μm core, VIS/NIR (low OH) Ocean Optics fiber. Although this fiber is designed for emission sensing in the visible to near-infrared range quantum efficiencies of up to 5% persist into the infrared range of interest. The fiber was mounted perpendicular to the coil axial direction pointing toward the center of the discharge tube. Figure 3 provides further clarification of this orientation. Difference turret orientations were used between gases to provide a frequency band of interest for each. As a result re-calibration via known wavelengths was performed at each orientation to ensure accurate spectra.

C. Vacuum Facility

The MPX cylindrical tube is connected end to end with that of a much larger cylindrical test chamber of length 3 meters and diameter 1.8 meters. During backfill to operational pressures MPX is isolated using an aluminum plate attached to a modified translation stage located within the large main chamber. This was done to provide the most static and repeatable gas conditions available to the authors. When sealed the MPX tube maintains a vacuum of less than 0.1 mTorr. Facility base pressure is around 0.01 mTorr.

III. Experimental Results

A. Raw Spectral Data

MPX discharges were performed on argon and xenon gases, separately at pressures of 10, 30, 50, and 100 mTorr back-filled from the isolated MPX quartz tube at less than 0.1 mTorr. Two different spectral data sets were acquired at each of these pressures for each gas. The first set were long-exposures of 20 μs to capture all dominant plasma activity over the entire discharge. Four to five of these spectra were acquired to verify consistency. Figures 4 (argon) and 5 (xenon) show the results of these long-exposures for each pressure. Vertical (intensity) scales for graphs (a)-(d) in each figure, though not shown, are of equal scale. The second set of data obtained was to provide a time-resolved intensity profile. These were captured at fixed CCD gate

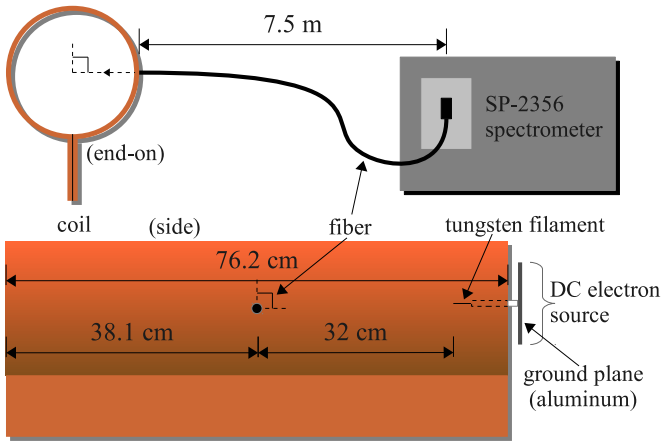

Figure 3. Optical fiber and DC source orientation.

widths of 250 ns each and gate delays starting from approximately the initial trigger, t_0 (actually $t = t_0 + 30$ ns due to OES controller delay). Thus time-marching a viewing window of 250 ns forward to build the time-resolved profile. At each delay between two and five spectra were acquired depending on whether or not plasma activity was observed. Multiple spectra per delay time were acquired to allow for post-process correction of temporal jitter (found to be upwards of 200 ns) inherent in the spark-gap switch. The switch used was particularly susceptible to jitter due to operation at 15 kV which is less than 50% of its 36 kV maximum rating. This process allowed for the re-construction of a nearly continuous time-resolved profile of light intensity during discharge. To elaborate, if three 250 ns exposures were taken at a preset delay of 2μs and the jitter times found post-process for these three shots were -100, 0, and +100 ns, respectively, then actual delay times of 2 - 0.1, 2, and 2 + 0.1 μs were observed. While it was common in previous studies to see no significant plasma activity until approximately the first 'zero-crossing' of the current,[9] the addition of a DC glow discharge has enabled earlier formation and observation of plasma as current initially increases at $t = t_0 + 2$ μs.

Four argon lines were used in analysis. Namely 696.5, 750.4, 794.8, and 801.5 nm. These were the focus of work by Iordanova and Koleva,[10] in which a cross-point method was used to estimate both electron temperature and density via intensity ratio pairs. Figure 6 shows raw intensity data (points) in addition to a smoothed least-squares trendline (curves) overly time-resolved for the argon 696.5 nm line for each pressure. Due to a technical issue the 10 and 30 mTorr argon data extend to only 7 and 5 μs, respectively. The wavelength bandwidth during argon testing was 695.6 to 833.5 nm.

Six of the eight IR xenon transition lines reported in Chiu *et al.*[11] were measured in this experiment. Namely the 823.2, 828.0, 834.7, 881.9, 904.5, and 916.3 nm transition lines. Their approach was to take the ratio of intensity of each of these lines over that of the 828 nm line and compare with equilibrium statistical calculation based on apparent collision cross-sections. The 823.2 nm line (referred hereto as the 823 line) representing the $2p^6$ to $1s^5$ transition (in Paschen notation) proved to be the most reliable due to high signal-to-noise ratio (SNR). Thus, for brevity, only the 823 to 828 intensity ratio is of focus for the work presented here. Figure 7 shows raw intensity data (points) as well as a smoothed least-squares trendline (curves) overly time-resolved for the xenon 823 line for each pressure. Smoothed trendlines were used to provide a cleaner look at the general trend as well as in the ratio calculations for electron temperature estimation. The wavelength bandwidth for CCD sensing during xenon testing was 803.8 to 937.7 nm.

B. Data Analysis

After initial testing at 10 mTorr argon a 3 to 5 shot 'cleansing' procedure was found to be necessary to remove contaminant spectra from the data after any re-pressurization to atmosphere. Evidence of this necessity can be seen in Fig. 4 where a strong peak is observed at 777 nm. This peak is believed to be most likely an atomic oxygen line.[12] Such a phenomenon has been encountered before in inductive plasmas and is generally thought to be the result of oxygen deposition to the inner quartz chamber walls. This cleansing

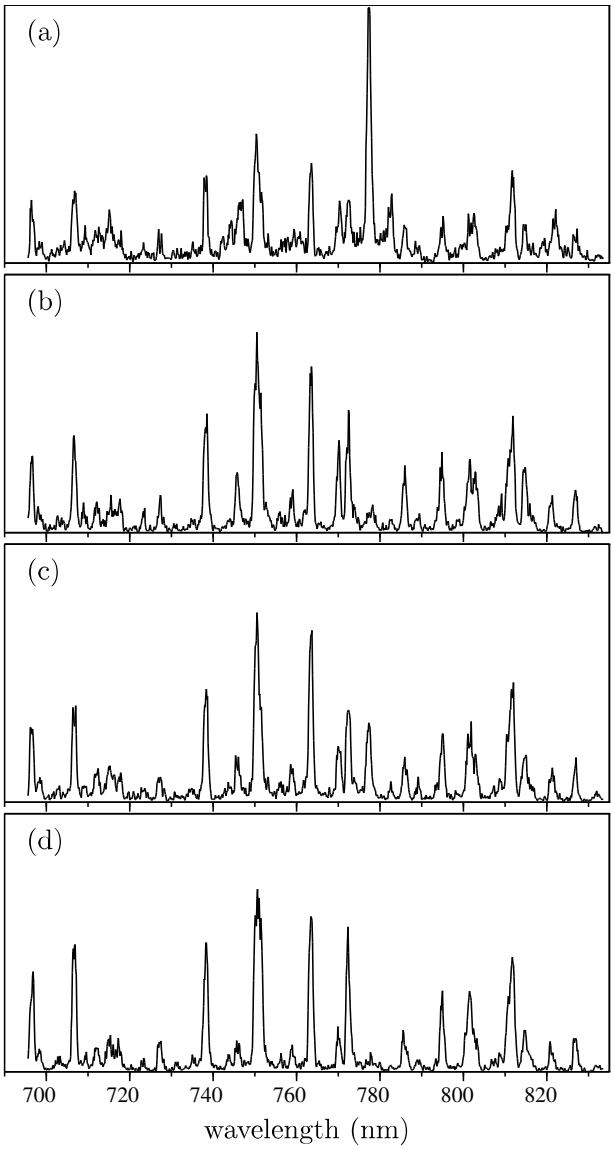

Figure 4. 20 μs MPX discharge exposures for argon at; (a) 10, (b) 30, (c) 50, and (d) 100 mTorr.

procedure was used for all subsequent pressures and gases.

Upon inspection of xenon data several strong lines were found that did not correspond to any wavelengths expected in first order xenon emission. However after some investigation all dominant lines observed in the infrared band were accountable by including 2^{nd} order diffraction from ionized Xe species transitions. Observed xenon UV spectra are cross-referenced with the National Institute of Standards and Technology (NIST) spectral database from which the dominant lines are attributed to transitions from singly ionized xenon species, Xe II. Second order Xe II lines and dominant Xe I lines are within less than 0.1% of NIST data with the exception of a peak at 935.3 nm. This single exception is attributed to the curve fit used in wavelength calibration of the CCD array. This analysis provided the verification that MPX cylindrical tube isolation provided a sufficiently contaminant-free environment. A more in-depth review of this analysis has been made previously by the authors.[13] In contrast, inspection of argon spectra yielded no such evidence of 2^{nd} order diffraction. Additionally, it can be seen by inspection of Figs. 6 and 7 that both time-resolved least-squares fits show an approximately 1/2 μs delay of spectral activity at a pressure of 10 mTorr.

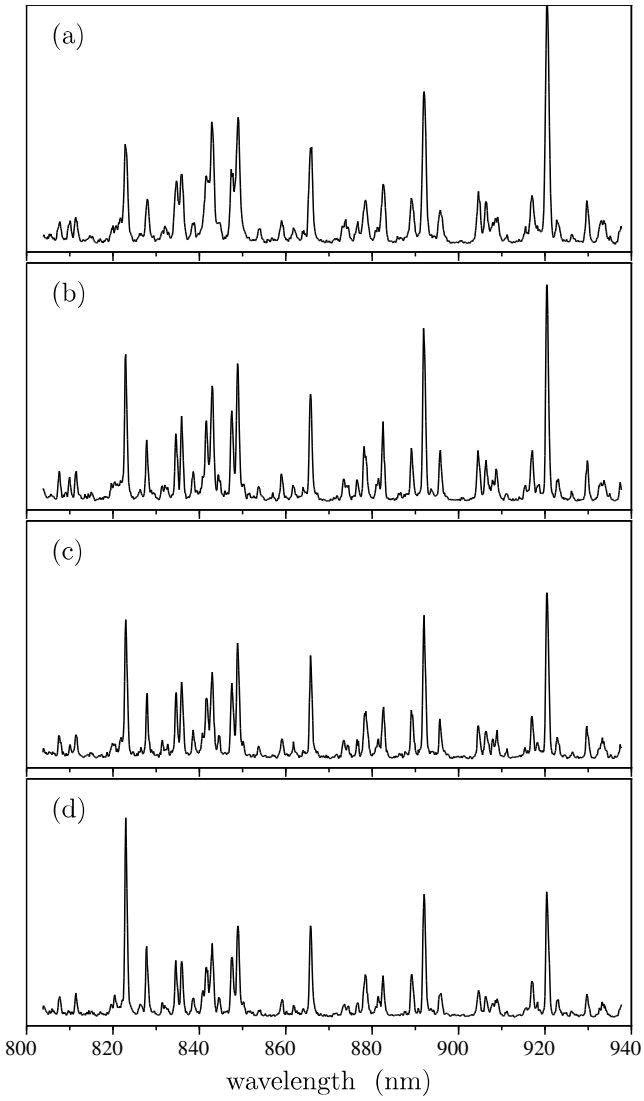

Figure 5. 20 μs MPX discharge exposures for xenon at; (a) 10, (b) 30, (c) 50, and (d) 100 mTorr.

IV. Numerical Analysis

A. Collisional-radiative Models

Seperate CR models were used in the estimation of electron temperature for each gas. For argon the model proposed by Iordanova and Koleva,[10] which utilizes the collisional statistics of the ground state as well as the first two excited levels (4 from $1s_{5-2}$ and 10 from $2p_{10-1}$) for neutral argon, approximates electron temperature and electron density via a *"cross-point"* method of analyzing intensity ratio pairs as outlined in that work. The Iordanova and Koleva (IK) model consists of 14 steady-state rate equations of the aforementioned excited species population densities. Effects to population density include electron impact ground state excitation (and de-excitation via the principle of detailed balance) and electron impact within the $1s_{5-2}$ levels, superelastic electron collisions which lead to metastable states, and electron collisions and collisions between heavy particles leading to $Z = 1$ ionization. Also diffusion to the walls of metastable $1s_5$ and $1s_3$ species and reduced (effective) radiative decay of resonance $1s_4$ and $1s_2$ species as well as of the upper $2p$ species via an escape factor calculation is included. Effective radiative decay is outlined in Ref. 10 and is defined as $A^{eff} = A_{2,1}\eta$ where $A_{2,1}$ is the transition probability from state $2 \rightarrow 1$ and η is the escape factor ($= 0 \rightarrow 1$).

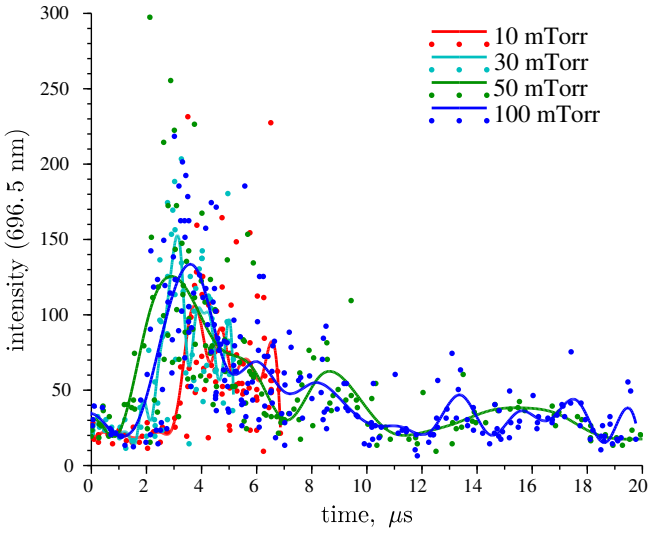

Figure 6. Time-resolved data for the argon 696.5 nm line at each of the four pressures tested in this work along with smoothed least-squares fits overlaid.

For xenon electron temperatures are approximated via the traditional intensity ratio method by estimates using the Karabadzhak *et al.*[14] collisional-radiative model (KCD model). The KCD model utilizes experimentally obtained cross-section data[11,15,16] in the calculation of neutral excited species populations via collisions with electrons, singly ionized (Xe^+), and doubly ionized (Xe^{2+}) xenon atoms. Endorsed by the authors of the original KCD model, xenon cross-sections for direct neutral excitation from Fons and Lin,[16] were used here to extend the applicability of the model from collisional energies of 70 eV to 150 eV. The data of Fons and Lin undergo both a zero-pressure correction and an optical opacity correction as outlined in Karabadzhak *et al.*[14] Electrons are assumed Maxwellian while $Z = 1, 2$ ion velocities are necessary and user-specified in the calculation of rate coefficients for those species, k_1 and k_2, respectively. Due to limited knowledge of ion velocities inside the pulsed plasma a first approximation of 3400 m/s estimated by Lorentz' Law, Faraday's Law, and the assumption of an ideal solenoid (i.e., $B(t) = \mu_0 n I(t)$) is used for the singly-ionized species. As supported in HET publications the KCD model assumes approximately double

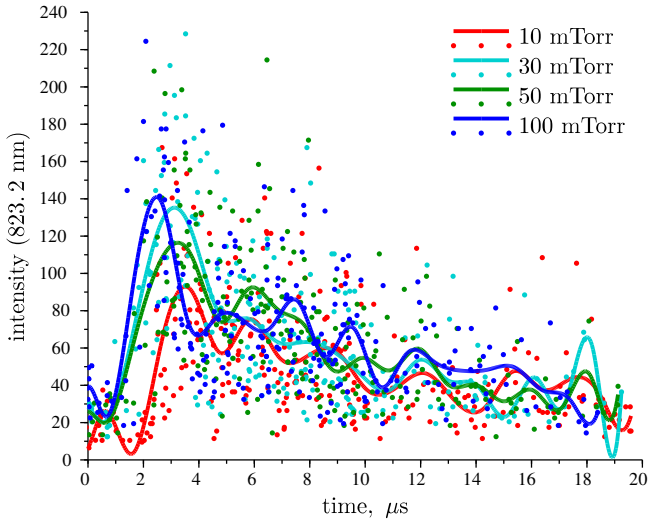

Figure 7. Time-resolved data for the xenon 823.2 nm line at each of the four pressures tested in this work along with smoothed least-squares fits overlaid.

the energy of the doubly-ionized species over the singly-ionized. This assumption is applied here as well. An auxiliary study of the KCD model revealed only very slight dependence on ion velocity in the range 1000 to 10,000 m/s. Line intensity per unit volume for a given wavelength is then approximated by,

$$J_\lambda(\text{Xe I}) = \frac{hc}{4\pi\lambda} N_0 N_e \left(k_e^\lambda + \alpha \cdot k_1^\lambda + \frac{1-\alpha}{2} k_2^\lambda \right) B^\lambda \tag{1}$$

where N_0 and N_e are the number densities of all xenon atoms and electrons, respectively. k_1 and k_2 are the emission excitation rate coefficients for impact between neutrals and Xe^+, Xe^{2+}, respectively, and $\alpha = N_1/N_e$. In all studies performed here the charge-state parameter, α is taken to have a value of 0.77. The parameter, B^λ, in Eq. 1 represents a correction factor as defined in Karabadzhak *et al.* and is dependent on the $1s_5$ metastable population.

In summary the fundamental difference between the two CR models is that while Iordanova and Koleva incorporate all of the inter-level and intra-level collisions of the first two argon excited state levels, Karabadzhak *et al.* avoid this complication while maintaining reasonable accuracy through *apparent* cross-sections for xenon. Both of these models assume a steady-state equilibrium condition of electron transfer processes. Given the pulsed nature of the MPX device the applicability of these models to it could certainly be argued. In addition, considerable efforts have been made by others in PIP research to show the development of energy 'modes' in electron energy distributions of these devices, arguing for a single or multi-peaked high energy distribution and against the often assumed (this work included) Maxwellian one.

B. Temperature Approximations

Analysis of each of the 20 μs exposure spectra shown in Figs. 4 and 5 are provided in Table 1. Using the IK model with conditions of this research an atypical result arose wherein two solutions were obtained for N_e and T_e. However electron temperature, T_e, which is of primary interest in this study only differed by 8.6% on average between solutions. The table shows that argon electron temperature varied between 3.32 and 3.57 eV for 50 and 10 mTorr, respectively. An omission is seen for 100 mTorr electron temperature due to an inability to converge in a cross-point solution for that pressure input. Currently the as-yet unknown reason for this lapse in a solution is being investigated. Incidentally, time-resolved T_e estimation for argon discharges is on-going.

For xenon, KCD model intensity ratio vs. T_e tabulated data is linearly interpolated and used to estimate electron temperature. From Table 1 T_e can be seen to range from 6.5 to 11.3 eV for xenon. From Fig. 7 an area of increased intensity can be seen from around 2 to 8 μs. Figure 8a shows time-resolved temperature estimates in this region of interest with the KCD model using the 823 to 828 line ratio and assuming a 2.0% tolerance against the models predicted ratios. Ratio tolerance with the model refers to how much percentage error an experimental derived ratio may have relative to a predicted ratio from the KCD model. The electron temperature quoted then is the average temperature from the range tabulated by the model within that tolerance. The temperature profiles in Figure 8 stem from the smoothed, time-resolved intensity data described in Section IVA and shown in Fig. 7. Figure 8b shows a coil discharge profile in the same time frame for reference. Electron temperature estimates in the time frame shown range nearly the entire scope of the model from 9 eV in 50 mTorr at 7.25 μs up to 92 eV in 10 mTorr at 2.4 μs.

Table 1. Electron temperature approximations for MPX at discharge voltage and frequency of 15 kV and 460 kHz, respectively, based on the xenon 823.2 to 828.0 nm ratio in the 20 μs (long-exposure) spectra of Fig. 5.

Pressure (mTorr)	Ar:$(\frac{697}{750} : \frac{802}{795})_{20\mu s}$	$T_{e,IK}$ (eV)	Xe:$(\frac{823}{828})_{20\mu s}$	$T_{e,KCD}$ (eV)
10	0.440 : 0.956	3.57	2.8	6.5
30	0.403 : 1.02	3.38	2.2	10.0
50	0.420 : 1.01	3.32	2.1	11.3
100	0.496 : 1.15	-	2.6	7.2

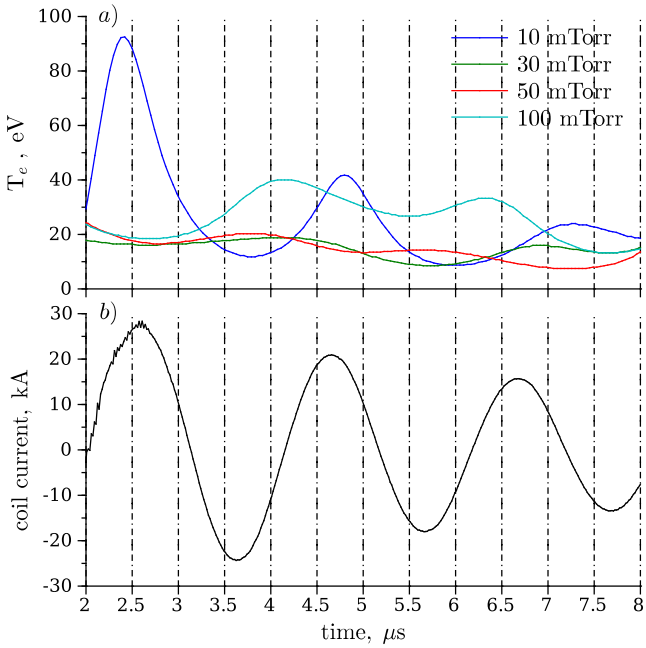

Figure 8. (a) MPX electron temperature estimates based on the Karabadzhak *et al.* model and ratio analysis of 823.2 nm to 828 nm lines from 2 to 8 μs. (b) typical coil current discharge profile during the same time frame.

C. Discussion

Table 1 provides temperature estimates based on the averaged 20 μs accumulations. The line ratio methods used in this work can be very susceptible to error in a low SNR environment. Inspection of Figs. 4 and 5 yields SNR values of 9.5 and 5 for the 823.2 and 828 lines, respectively, for the long-exposure spectra. In contrast the short exposures of 250 ns had typical SNR values ranging from less than 2.5 up to 5. Thus electron temperature estimates based on the long-exposures should be considered the more accurate while realizing that these temperatures would represent integrated activity over the entire discharge.

From Fig. 8 two observations are made. First is the presence of high electron temperature peaks during the 10 mTorr operating pressure that approximately coincide with current peaks around 2.5 and 4.75 μs. These peaks in estimated electron temperature are within the realm of those reported for PIP devices.[17,18] However, they are clearly unique in comparison with the other three pressures tested. This is partially attributed to the substantial delay in radiative activity at 823.2 nm in the 10 mTorr case compared to the other three pressures. This can be observed by returning to Fig. 7. In Fig. 7, a ramp-up in line intensity can be seen just after 1 μs in the 30, 50, and 100 mTorr studies. In contrast, line intensity at 10 mTorr does not show a similar ramp until approximately 2 μs. Furthermore, a similar investigation of the 828 nm line intensity revealed that this same delay was present. Additionally rate of change of the 828 nm line intensity just after 2 μs was found to be greater in the 10 mTorr case driving the ratio down and estimated electron temperature up.

Second, nearly all time-resolved temperature values shown in Fig. 8 (for $2 \leq t \leq 8$ μs) are greater than those given in Table 1 (for a total discharge of 20 μs). While the part of low SNR that contributes to poor ratio calculations and temperature estimations has been emphasized above and is again mentioned here as a source of error, it should also be noted that some temperature estimations (particularly the 30 and 50 mTorr data) do not fall far from the long-exposure estimates. Table 1 reports estimates of 10.0 and 11.3 eV for 30 and 50 mTorr, respectively. In the temporal region of interest shown in Fig. 8 electron temperatures range between 9 and 24 eV for these two pressures given a ratio tolerance with the model of 2% as outlined above. However, for a ratio tolerance of 20% and using the lowest temperature within this tolerance the range decreases to between 6.4 and 12.4 eV for 30 mTorr and 5.3 and 15.7 eV for 50 mTorr.

V. Conclusions

IR and UV spectra were acquired for a pulsed theta-pinch xenon plasma at 10, 30, 50, and 100 mTorr. The IR band, specifically the most intense transition lines of 823.2 and 828.0 nm from the $2p$ to $1s$ sub-shells, were utilized for a line ratio technique to estimate electron temperature. Lines unaccountable by 1^{st} order Xe I transitions in the IR band were accountable by 2^{nd} order Xe II transitions observed in the UV band. The collisional-radiative model developed by Karabadzhak *et al.* to describe Hall-effect thrusters was used to estimate electron temperatures from the a fore mentioned line ratio. Total discharge spectra yield temperatures ranging from 3.32 eV for argon to 11.3 eV for xenon. High noise fast spectra (CCD gate width = 250 ns) yield time-resolved temperatures ranging from 9 to 92 eV for a 2% tolerance against the model. Time-resolved electron temperature estimations for the 30 and 50 mTorr cases yield the most stable and closest agreement with the more accurate integrated spectra estimations.

Acknowledgments

We would like to thank Dr. Scott Kovaleski at our sister campus; University of Missouri-Columbia, for the use of his OES equipment that made this work possible. AFOSR for their continued funding (award# FA9550-10-1-0204). Dr.'s Dan Brown and Carrie Hill at AFRL for their continued input and suggestions regarding theta-pinch concepts. Dr.'s Jean-Luc Cambier and Ben Prince at AFRL for their advice on emission spectroscopy. Dr. Snejana Iordanova at the Sofia University of Bulgaria for her help in re-creating her collisional-radiative model. And Dr. Bill Hargus and 1^{st} Lt. Ashley Gonzales (AF) for providing their rendition of the base KCD model code.

References

[1]Sakuta, T., Oguri, S., Takashima, T., and Boulos, M. I., "Effects of plasma diameter and operating frequency on dynamic behavior of induction thermal plasma," *Plasma Sources Sci. Technol.*, Vol. 2, 1993, pp. 67–71.

[2]Polzin, K. A., "Scaling and Systems Considerations in Pulsed Inductive Plasma Thrusters," *IEEE - Transactions on Plasma Science*, Vol. 36, No. 5, Oct. 2008, pp. 2189–2198.

[3]Werner, Z., Piekoszewski, J., and Szymczyk, W., "Generation of high-intensity pulsed ion and plasma beams for material processing," *Vacuum*, Vol. 63, No. 4, Aug. 2001, pp. 701–708.

[4]Wurden, G., "FRCHX Magnetized Target Fusion HEDLP Experiments," *IC/P4-13*, IAEA, Geneva, Switzerland, Oct. 2008.

[5]Kirtley, D., Slough, J., Pfaff, M., and Pihl, C., "Steady Operation of an Electromagnetic Plasmoid Thruster," *8th MSS/5th LPS/5th SPS Joint Subcommittee Meeting*, Dec. 2011.

[6]Pahl, R. A. and Rovey, J. L., "Pre-Ionization Plasma in a FRC Test Article," 50th Aerospace Sciences Meeting, AIAA, Nashville, TN, 2012.

[7]Pahl, R. A., Meeks, W. C., and Rovey, J. L., "Magnetic Field Mapping of a Field Reversed Configuration Test Article," 47th Joint Propulsion Conference & Exhibit, AIAA, San Diego, CA, 2011.

[8]Polzin, K., Rose, M., and Miller, R., "Operational Characteristics of a Low-Energy FARAD Thruster," American Institute of Aeronautics and Astronautics, July 2008.

[9]Meeks, W. C. and Rovey, J. L., "On the delayed gas breakdown in a ringing theta-pinch with bias magnetic field," *Physics of Plasmas*, Vol. 19, No. 5, 2012, pp. 052505.

[10]Iordanova, S. and Koleva, I., "Optical emission spectroscopy diagnostics of inductively-driven plasmas in argon gas at low pressures," *Spectrochimica Acta Part B: Atomic Spectroscopy*, Vol. 62, No. 4, April 2007, pp. 344–356.

[11]Chiu, Y.-h., Austin, B. L., Williams, S., Dressler, R. A., and Karabadzhak, G. F., "Passive optical diagnostic of Xe-propelled Hall thrusters. I. Emission cross sections," *Journal of Applied Physics*, Vol. 99, No. 11, June 2006, pp. 113304–113304–11.

[12]Krstulovi, N., Labazan, I., Miloevi, S., Cvelbar, U., Vesel, A., and Mozeti, M., "Optical emission spectroscopy characterization of oxygen plasma during treatment of a PET foil," *Journal of Physics D: Applied Physics*, Vol. 39, No. 17, Sept. 2006, pp. 3799.

[13]Meeks, W. C. and Rovey, J. L., "Optical Emission Spectroscopy of Plasma Formation in a Xenon Theta-Pinch," *IEEE Transactions on Plasma Science*, *(submitted for review Sept. 2013)*.

[14]Karabadzhak, G. F., Chiu, Y.-h., and Dressler, R. A., "Passive optical diagnostic of Xe propelled Hall thrusters. II. Collisional-radiative model," *Journal of Applied Physics*, Vol. 99, No. 11, June 2006, pp. 113305–113305–12.

[15]Sommerville, J., *Emission Cross Sections for Neutral Xenon Impacted by Xe+ and Xe2+*, Ph.D. thesis, Michigan Technological University, 2006.

[16]Fons, J. T. and Lin, C. C., "Measurement of the cross sections for electron-impact excitation into the 5pˆ{5}6p levels of xenon," *Physical Review A*, Vol. 58, No. 6, Dec. 1998, pp. 4603–4615.

[17]Zhang, S., Wurden, G., Intrator, T., Ruden, E., Waganaar, W., Grabowski, C., Renneke, R., and Degnan, J., "High-

density field-reversed configuration plasma for magnetized target fusion," *IEEE Transactions on Plasma Science*, Vol. 34, No. 2, 2006, pp. 223–228.

[18]Kronast, B., Rhr, H., Glock, E., Zwicker, H., and Fnfer, E., "Measurements of the Ion and Electron Temperature in a Theta-Pinch Plasma by Forward Scattering," *Physical Review Letters*, Vol. 16, No. 24, June 1966, pp. 1082–1085.